INTL JOURNAL OF ELECTRONICS AND TELECOMMUNICATIONS, 2023, VOL. 69, NO. 3, PP. 469-473
Manuscript received June 7,2023; revised July, 2023. DOI: 10.24425/ijet.2023.146494

Design of a Novel 1x4 Two-Dimensional Demultiplexer Based on Multicore Photonic Crystal Fiber

Assia Ahlem Harrat, Mohammed Debbal, and Mohammed Chamse Eddine Ouadah

***Abstract*—This work suggests a brand-new 1*4 two-dimensional demultiplexer design based on multicore photonic crystal fiber. Numerical models show that the optical signals can be separated in a photonic crystal fiber construction using optical signals with wavelengths of 0.85, 1.1, 1.19, and 1.35 µm injected on the center core and separated into four cores. The innovative design switches different air-hole positions using pure silica layers throughout the length of the fiber to regulate the direction of light transmission between layers.**

Wavelength demultiplexers are essential parts of optical systemic communications. They serve as a data distributor and can use a single input to produce multiple outputs. The background material is frequently natural silica, and air holes can be found anywhere throughout the length of the fiber as the low-index components.

The simulation results showed that after a 6 mm light propagation, the four-channel demux can start to demultiplex.

***Keywords*—Photonic Crystal Fiber; demultiplexer; light coupling; normalized power; light transmission**

I. Introduction

A NEW family of optical waveguides known as photonic crystal fibers (PCFs) has recently received significant research and commercial interest [1-3]. PCFs are silica or polymer microstructured waveguides with plenty of air holes positioned in the cladding area of the fiber [4]. In PCFs, light can be steered either by the photonic band gap (PBG) phenomena [5, 6] or through the effective index mechanism connected to the modified total internal reflection (MTIR) [7, 8]. The propagation characteristics of PCF can be fine-tuned, offering additional functions, by adding other gases, liquids, or solid materials into the air holes [9-13].

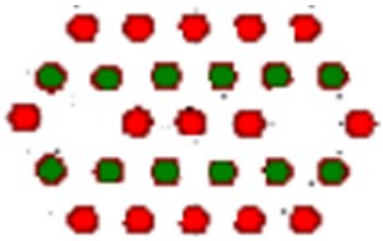

Fig. 1. Photonic Crystal Fiber Structure

Air holes in the cladding area are evenly distributed around a core defect zone to create PCFs [14, 15]. The dimensions of the PCF structure are shown in Figure 1; where d stands for the diameter of the air holes and ʌ (pitch) represents the separation between them. When pure silica is used as the background material, lower-index zones are created by evenly spacing air holes throughout the length of the fiber. The parameters of the structure are shown in Table I, and the refractive index of silica for the selected wavelength (0.85, 1.1, 1.19, and 1.35 µm) are shown in Table II.

TABLE I
THE PARAMETER OF THE PCF

Parameter	Value
Pitch (ʌ)	1.88 (µm)
Diameter (d)	0.9 (µm)
Length of fiber (Z)	6000 (µm)
n_{air}	1

TABLE II
THE REFRACTIVE INDEX OF SILICA OF THE FOUR SELECTED WAVELENGTH

λ (µm)	n_{silica}
0.85	1.4525
1.1	1.4492
1.19	1.44816
1.35	1.44635

An electronic device called a demultiplexer divides a multiplex signal into its constituent parts. It is one among the numerous components that go into creating wavelength division multiplexing (WDM) systems [16] and allows the signal carried by several wavelengths to be split between a single input and multiple outputs. High data bitrate transfer, low propagation bitrate, and low bit error rate are just a few benefits of using this device. [17-20].

Assia Ahlem Harrat and Mohammed Debbal are with the Department of Electronics and Telecommunications, Faculty of Science and Technology, University of Belhadj Bouchaib, Algeria (e-mail: harrat22.ahlem@gmail.com, debbal.mohammed@gmail.com).

Mohammed Chamse Eddine Ouadah is with the Department of Telecommunications, Faculty of Electrical and Computer Engineering, University of Mouloud Mammeri, Algeria (e-mail: ouadahc@gmail.com).

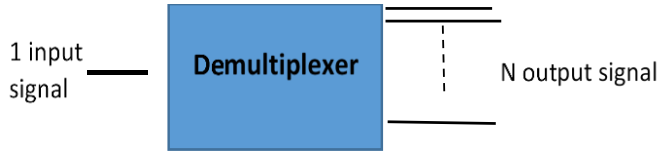

Fig. 2. Example of demultiplexer device

There have been numerous reports of Demux based on photonic crystal fiber. They have put out a brand-new design for an RGB demultiplexer that is based on a polycarbonate (PC) MC-POF structure. This design enables to control of the direction of light propagation between the PC layers by replacing different air-hole locations with PC layers along the fiber length [18], then it has been demonstrated that a novel eight-channel demux device based on multicore photonic crystal fiber (PCF) architectures that operate in the C-band region (1.530-1.565 µm) is feasible [9], Siahlo et al made a photonic crystal fiber with a zero-dispersion wavelength at 1.552 µm is used as the nonlinear medium in a nonlinear optical loop-mirror-based demultiplexer [21], Hameed et al analyzed and proposed a novel multiplexer-demultiplexer (MUX-DEMUX) design based on index-guiding soft glass nematic liquid crystal (NLC)-based photonic crystal fiber coupling [22].

By adopting various air-hole sizes in the PCF structure and altering the PCF index profile by replacing certain air-hole areas with pure silica throughout the fiber length, this work illustrates the capability of linking light across closed ports (cores) in a PCF design. The simulation results showed that after 6mm of light propagation, the four-channel demux could be demultiplexed.

II. Materials and Methods

The two-dimensional (2D) demultiplexer design for the multicore PCF is currently provided with a ratio of 1*4.

The primary function of the PCF demux device is to control the size of the light coupling length between two neighboring ports and to confine light inside the channel (core). To achieve these results, some air-hole actors can be replaced with a pure silica high-index substance running the length of the fiber.

Light can be coupled between two closer ports with the same index of refraction value, and a port with a high index value can also achieve significant light confinement (pure silica material) thanks to the MTIR (modified total internal reflexion), which is the basis for the light-guiding mechanism in our design.

The refractive index profile of the suggested structure at y = 0mm is shown in Figure 3 (a).

In this diagram, the purple portions represent air (n=1) while the red areas indicate pure silica (n=1.45). Figure 3 (b) shows the cross sections of the suggested demultiplexer at z=0mm, the plane from which light propagates, and Figure 3 (c) shows that there are four cores at z=6mm. Port 1 represents output channel 1, port 3 represents channel 2, port 5 represents output channel 3, and port 8 represents output channel 4.

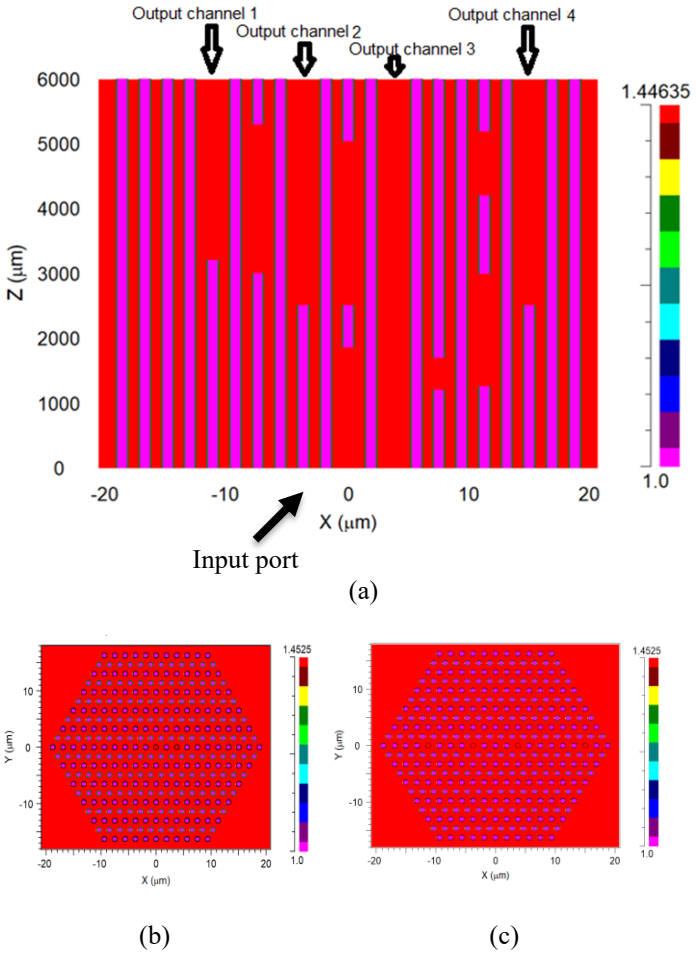

Fig. 3. The cross-section of the 1*4 wavelength demux: (a) XZ plane at y = 0 mm. (b) XYPlane at z = 0 mm. (c) XY plane at z = 6mm

III. Results

Figures 4 and 5 show the input/output beam at the x-y plane for the four wavelengths of 0.85, 1.1, 1.19, and 1.35 µm. The power demultiplexer had an effect since, after 6mm, we noticed that our input signal had been divided into four output signals.

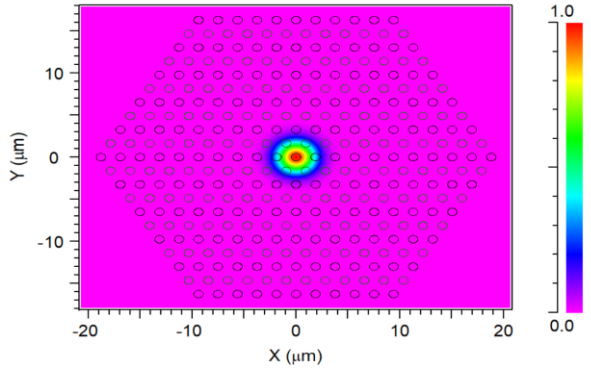

Fig. 4. The 1x4 input power demultiplexing of the four optical signals (a: λ=0.85µm; b: λ =1.1µm; c: λ=1.19µm; d: λ=1.35µm) at z=0mm

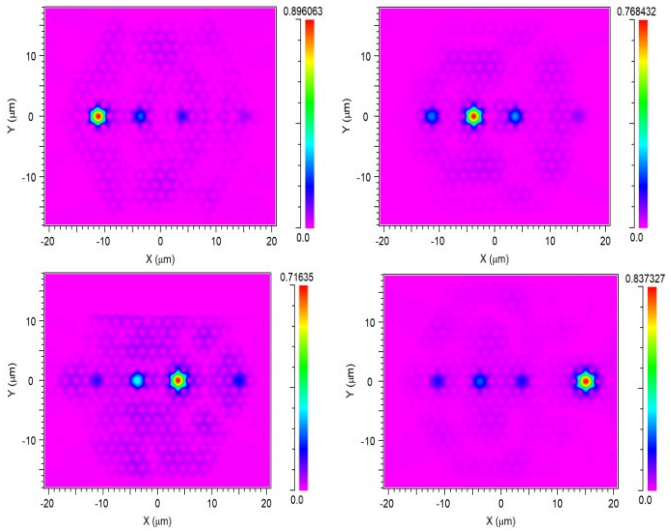

Fig. 5. XY cross-section optical signals simulations intensity demultiplexing 1*4 (a: λ=0.85µm; b: λ =1.1µm; c: λ=1.19µm; d: λ=1.35µm) at z=6mm

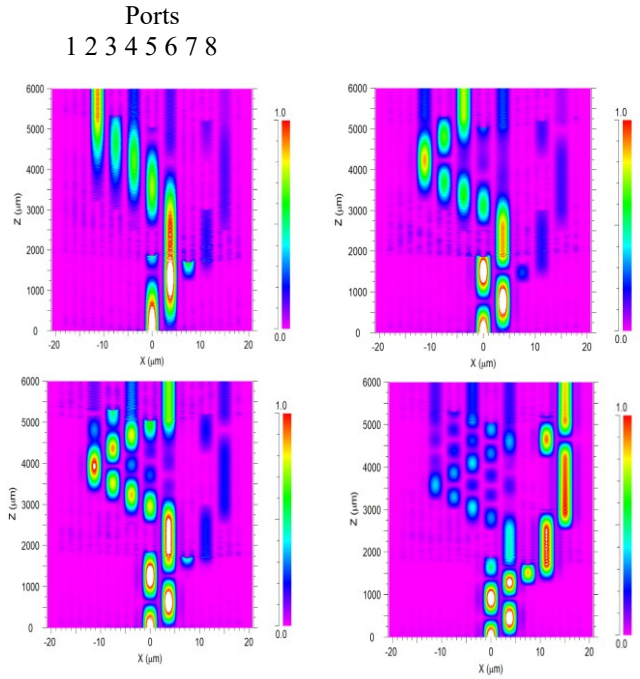

Fig. 6. Profile of intensity of the 1*4 wavelength demultiplexer. a: for the optical signal λ =0.85µm; b: λ = 1.1µm; c: λ =1.19µm; c: λ = 1.35µm

Figure 6 shows the light coupling between PC cores and the light traveling across the entire fiber length at the x-z plane for the chosen wavelength channels.

The optical path of the light with a wavelength of 0.85 µm in the PCF structure is shown in Figure 6 (a) as follows: The first z step occurs at z=1.41 mm, where the light is directed from the input port 4 toward the output port 5; the second z step occurs at z=4.116 mm, where the output channel 1 is the intended recipient of the light traveling through the coupled port 4. Finally, the light arrives on port 2 at z=5.346 mm, and passes from port 4 to port 3 at 4.8 mm and from port 3 to 2 at 4.8 mm, before propagating to the output port 1 (channel 1).

Figure 6 (b) depicts the optical path taken by light with a wavelength of 1.1 µm through the PCF structure. The light is directed from the input port 4 toward the output port 5 in the first z step, which happens at z=2 mm. In the second z step, which happens at z=3.421 mm, the light is destined for the output channel 2 but is passing through the coupled port 4. At z=5.356 mm, the light propagates to the output port 1 (channel 2) after passing from port 4 to port 3, port 3 to 2 at 3.7 mm, port 2 to port 1 at 4.2 mm, and port 1 to 2 at 5 mm.

In Figure 6 (c), the optical path of light with a wavelength of 1.19 µm in the PCF structure is depicted as follows: The first z step happens at z=2 mm, where light is directed from the input port 4 toward the output port 5, and the second z step occurs at z=3.321 mm, where light passing through the coupled port 4 is destined for the output channel 3. Before reaching the output port 5 (channel 3), the light arrives on port 4 at z=5 mm and travels from port 4 to port 3 at z=3.4 mm, port 3 to port 2 at 3.7 mm, port 2 to port 1 at 3.9 mm, port 1 to port 4 at 4.5 mm passing from port 2 and port 3 at 4.8 mm and 5.1 mm, respectively.

Figure 6 (d) illustrates the optical path of light in the PCF structure with a wavelength of 1.35 µm as follows: Light is directed from the input port 4 toward the output port 8 in the first z step, which occurs at z=1.398 mm. Light is directed toward the output channel 4 in the second z step, which happens at z=1.666 mm from port 5 to port 6. The light travels from port 6 to port 7 at z=1.785 mm, from port 7 to port 8 at 3 mm, then from port 8 to port 7 at 4.661 mm, and arrives at 5.1mm on port 7 before arriving at output port 8 (channel 4).

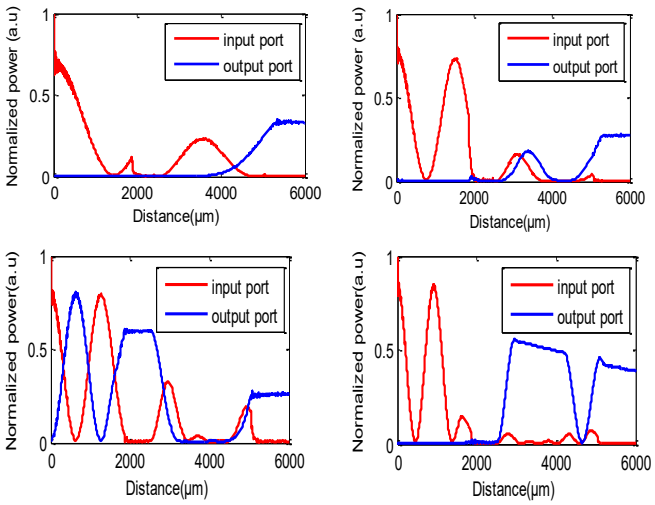

Fig. 7. Standardized input and output power of 1*4 power demultiplexer for the optical signals λ1=0.85µm, λ2=1.1µm, λ3=1.19µm, and λ4=1.35µm

Figure 7 (a) demonstrates that the input power in the core achieves a maximum of 76%; nevertheless, transmission losses of 24% were incurred because of connector loss, bends, and the absorption of the intrinsic materials. At 3.822mm, the output power begins to grow and reaches a maximum of 33% and the input power drops to zero.

The input power in the core peaks at 80% in Figure 7 (b) before decreasing to zero at 4511mm. To focus input power on the output port, which must travel through several stages as it connects one segment to its neighbor with light coupling, this is necessary. The output port power starts to increase at the same value of 4511mm and rises to a maximum of 27%.

At 0 mm, the initial power of the transmission is 80%, and we observed 20% transmission losses as a result of intrinsic material absorption, bends, and connection loss. However, after this point, the input signal will be zero because it is now pointing to the output port. To create a coupling zone and amplify our signal, we drilled silica holes through the at different phases. At the output port, power increases from 0% to 80%; at 5 mm, the output power is at its maximum of 25%, while the input power is at 0% (figure 7 (c)).

Figure 7 (d) shows that the input power peaks at 83% in the core and drops to zero at the departure point (0 mm). This is because the input power will be focused on the output port after passing through several stages while moving from one segment to its neighbor with light coupling. The output port power grows at 2.514mm and reaches a maximum of 50%; at 6mm, the output power is 39% and the input is at zero.

Our four optical signals are shown in Figure 8 at their initial maximum (100%). Figure 9 (a-d) showed a high transmission of 89% for the core (0.85 µm), 76% for the core (1.1 µm), 71% for the core (1.19 µm), and 83% for the core (1.35 µm), which is a successful outcome. At the output (6mm), the input signal was divided into four signals, which is the role of a demultiplexer.

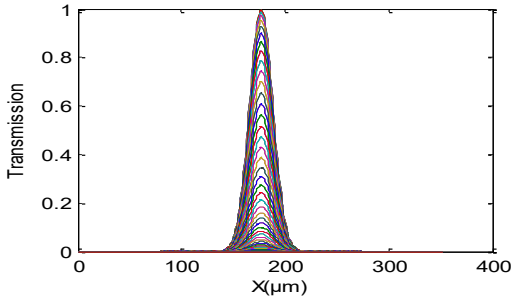

Fig. 8. The normalized coupling efficiency at z=0mm

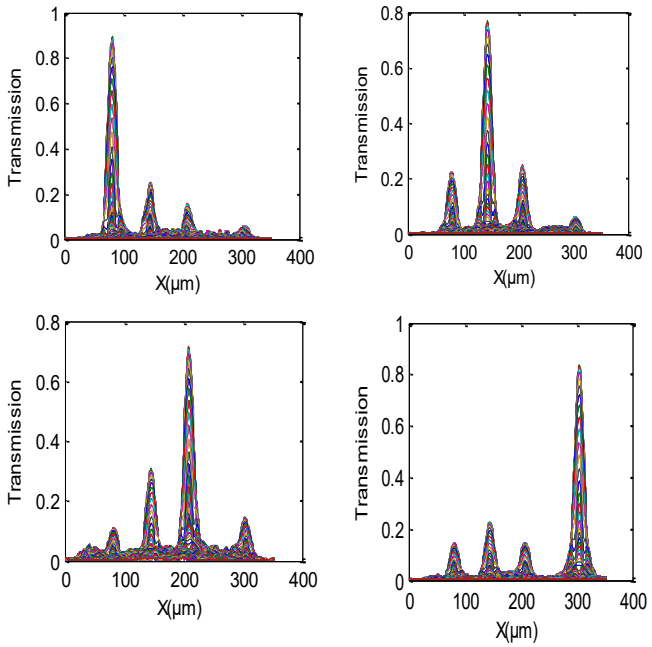

Fig. 9. The normalized coupling efficiency at z=6mm for the 0.85µm(a), (1.1µm(b), 1.19µm(c), 1.35µm(d)

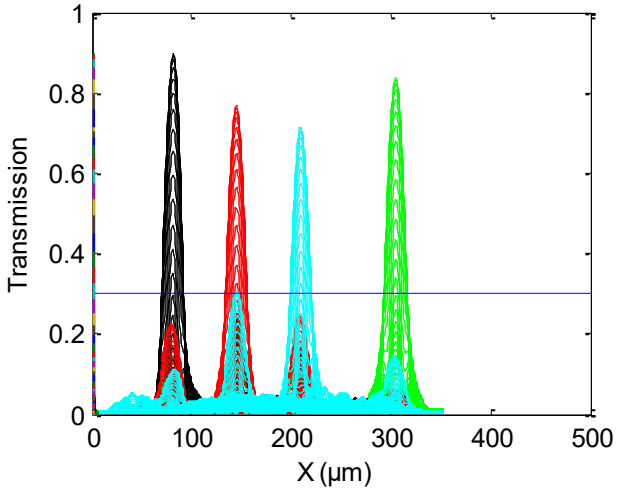

Fig. 10. The total normalized coupling efficiency at z=6mm for the four output optical signals

CONCLUSION

In conclusion, we have proposed a 1x4 wavelength demultiplexer in this work and demonstrated that this demultiplexer can be used with integrated multiple air-hole placements in the PCF structure and replaced along the PCF axis with pure silica and that will be routed until the output, to achieve the required optical power outputs at their highest level.

Additionally, this work demonstrates how the MTIR mechanism may be employed to alter the direction of light propagation within the multicore PCF, allowing light to couple only the silica components and achieving greater light confinement for the higher index material.

According to the simulation results, the 1x4 wavelength demultiplexer is capable of separating the four wavelengths effectively, allowing them to propagate through the device with minimal interference. This separation occurs after a distance of 6 mm and is achieved using integrated multiple air-hole placements within the photonic crystal fiber (PCF) structure. The demultiplexer can be further modified by replacing certain sections along the PCF axis with pure silica, ensuring that the required optical power outputs are achieved at their highest levels.

The output transmission for the four wavelengths (0.85 µm, 1.19 µm, 1.1 µm, and 1.35 µm) at their respective output ports is 89%, 76%, 71%, and 83%. These results demonstrate the potential of this device to be used in a Dense Wavelength Division Multiplexing (DWDM)-based optical communication system, which requires the transmission of multiple optical signals at different wavelengths over a single optical fiber. Overall, the 1x4 wavelength demultiplexer shows great promise for improving the performance of optical communication systems by providing effective separation of different wavelength channels.

REFERENCES

[1] N. A. Mohammed, O. E. Khedr, E.-S. M. El-Rabaie, and A. A. Khalaf, "Literature review: on-chip photonic crystals and photonic crystal fiber for biosensing and some novel trends," IEEE Access, 2022. https://doi.org/10.1109/ACCESS.2022.3170912

[2] V. S. Chaudhary, D. Kumar, B. P. Pandey, and S. Kumar, "Advances in photonic crystal fiber-based sensor for detection of physical and biochemical parameters-A review," IEEE Sensors Journal, 2022.

[3] B. Kaur, S. Kumar, and B. K. Kaushik, "Advances in photonic crystal fiber: sensing and supercontinuum generation applications," Optical Fiber Technology, vol. 72, p. 102982, 2022. https://doi.org/10.1016/j.yofte.2022.102982

[4] B. Drljača et al., "Theoretical Investigation of Bandwidth in Multimode Step-Index Silica Photonic Crystal Fibers," in Photonics, 2022, vol. 9, no. 4: MDPI, p. 214. https://doi.org/10.3390/photonics9040214

[5] P. Jaworski, "Molecular dispersion spectroscopy in a CO2-filled all-fiber gas cells based on a hollow-core photonic crystal fiber," Optical Engineering, vol. 58, no. 2, pp. 026112-026112, 2019. https://doi.org/10.1117/1.OE.58.2.026112

[6] M. Rachana, I. Charles, S. Swarnakar, S. V. Krishna, and S. Kumar, "Recent advances in photonic crystal fiber-based sensors for biomedical applications," Optical Fiber Technology, vol. 74, p. 103085, 2022. https://doi.org/10.1016/j.yofte.2022.103085

[7] I. K. Yakasai, P. E. Abas, S. Ali, and F. Begum, "Modelling and simulation of a porous core photonic crystal fibre for terahertz wave propagation," Optical and Quantum Electronics, vol. 51, pp. 1-16, 2019. https://doi.org/10.1007/s11082-019-1832-x

[8] A. A.-M. Bulbul, R. H. Jibon, S. Biswas, S. T. Pasha, and M. A. Sayeed, "Photonic crystal fiber-based blood components detection in THz regime: Design and simulation," Sensors International, vol. 2, p. 100081, 2021. https://doi.org/10.1016/j.sintl.2021.100081

[9] D. Malka and G. Katz, "An eight-channel C-band demux based on multicore photonic crystal fiber," Nanomaterials, vol. 8, no. 10, p. 845, 2018. https://doi.org/10.3390/nano8100845

[10] Y. L. Hoo, W. Jin, C. Shi, H. L. Ho, D. N. Wang, and S. C. Ruan, "Design and modeling of a photonic crystal fiber gas sensor," Applied Optics, vol. 42, no. 18, pp. 3509-3515, 2003. https://doi.org/10.1364/AO.42.003509

[11] I. Mired, M. Debbal, and H. Chikh-Bled, "Pressure Sensing Based on Photonic Crystal Fiber by Infiltrating the Air-Holes with Water," Progress In Electromagnetics Research C, vol. 130, pp. 69-82, 2023. https://doi.org/10.2528/PIERC22122503

[12] A. A. Harrat, M. Debbal, and M. C.-E. Ouadah, "1× 2 power splitter based on photonics crystals fibers," Journal of Optical Communications, no. 0, 2023. https://doi.org/10.1515/joc-2022-0273

[13] B. K. Paul et al., "Investigation of gas sensor based on differential optical absorption spectroscopy using photonic crystal fiber," Alexandria Engineering Journal, vol. 59, no. 6, pp. 5045-5052, 2020. https://doi.org/10.1016/j.aej.2020.09.030

[14] M. S. Hossain, M. Kamruzzaman, S. Sen, M. M. Azad, and M. S. H. Mollah, "Hexahedron core with sensor based photonic crystal fiber: An approach of design and performance analysis," Sensing and Bio-Sensing Research, vol. 32, p. 100426, 2021. https://doi.org/10.1016/j.sbsr.2021.100426

[15] F. A. Mou, M. M. Rahman, M. R. Islam, and M. I. H. Bhuiyan, "Development of a photonic crystal fiber for THz wave guidance and environmental pollutants detection," Sensing and Bio-Sensing Research, vol. 29, p. 100346, 2020. https://doi.org/10.1016/j.sbsr.2020.100346

[16] A. S. J. Choyon and R. Chowdhury, "Multifunctional chalcogenide (As2S3, As2Se3) dual-core photonic crystal fiber with elliptical air-hole for mid-IR optical communications: Design and analysis," Optik, vol. 258, p. 168857, 2022. https://doi.org/10.1016/j.ijleo.2022.168857

[17] P. D. Lakshmijayasimha, A. Kaszubowska-Anandarajah, E. P. Martin, and P. M. Anandarajah, "Optical linewidth tolerant mmW generation employing a dual-stage active demultiplexer," IEEE Photonics Technology Letters, vol. 34, no. 9, pp. 451-454, 2022.

[18] R. Dadabayev and D. Malka, "A visible light RGB wavelength demultiplexer based on polycarbonate multicore polymer optical fiber," Optics & Laser Technology, vol. 116, pp. 239-245, 2019. https://doi.org/10.1016/j.optlastec.2019.03.034

[19] S. Naghizade and S. Sattari-Esfahlan, "An optical five channel demultiplexer-based simple photonic crystal ring resonator for WDM applications," Journal of Optical Communications, vol. 41, no. 1, pp. 37-43, 2020.

[20] F. Mehdizadeh and M. Soroosh, "A new proposal for eight-channel optical demultiplexer based on photonic crystal resonant cavities," Photonic Network Communications, vol. 31, no. 1, pp. 65-70, 2016. https://doi.org/10.1007/s11107-015-0531-1

[21] A. I. Siahlo et al., "A high-speed demultiplexer based on a nonlinear optical loop mirror with a photonic crystal fiber," IEEE Photonics Technology Letters, vol. 15, no. 8, pp. 1147-1149, 2003. https://doi.org/10.1109/LPT.2003.815365

[22] M. Hameed, S. Obayya, and R. Wiltshire, "Multiplexer–demultiplexer based on nematic liquid crystal photonic crystal fiber coupler," Optical and quantum electronics, vol. 41, pp. 315-326, 2009. https://doi.org/10.1007/s11082-009-9334-x